Physical and Sensing Properties of Aluminum-Doped Iron (III) Oxide Thin Films Deposited via Chemical Spray Pyrolysis

Ameera Jwad Kadhm[1],Tahseen H. Mubarak[2], Reem Sami Ali[1], Shaymaa A. Hussein[3], Sami Salman Chiad[1], Nadir Fadhil Habubi[1,4,5] and Yassin Hasan Kadhim[6]

[1]*Department of Physics, College of Education, Mustansiriyah University, 10052 Baghdad, Iraq*
[2]*Department of Physics, College of Science, University of Diyala, 32001 Baqubah, Diyala, Iraq*
[3]*Department of Medical Laboratory Techniques, Al-Manara College for Medical Science, 62001 Al-Amarah, Iraq*
[4]*Department of Radiation and Sonar Technologies, Alnukhba University College, 10013 Baghdad, Iraq*
[5]*Department of Radiology Techniques, Al-Qalam University College, 36001 Kirkuk, Iraq*
[6]*Department of Optics Techniques, College of Health and Medical Techniques, AL-Mustaqbal University, 51001 Hillah, Babylon, Iraq*
dean@sciences.uodiyala.edu.iq, dr.sami@uomustansiriyah.edu.iq, nadirfadhil@uomustansiriyah.edu.iq, yassin.hasan@uomus.edu.iq, shaimaa2021@uomanara.edu.iq, amerajwad2017@gmail.com

Keywords: Aluminum-Doped Iron Oxide, Thin Film, CSP, XRD, AFM, Optical Properties, Sensitivity and Resistance.

Abstract: Fe_2O_3:Al (1–3 at%) thin films were successfully grown on glass substrates at 400°C using the chemical spray pyrolysis (CSP) technique. The X-ray diffraction (XRD) patterns confirmed the formation of α-Fe_2O_3 with a prominent (104) peak, indicating high crystallinity. The average grain size (D) increased from 15.82 nm to 18.70 nm with increasing Al content, while the lattice strain (ε) decreased from 2.18 to 1.85, suggesting improved crystal quality. Atomic Force Microscopy (AFM) analysis showed a reduction in surface roughness and uniform particle distribution, with particle diameters ranging from 65.5 nm to 52.31 nm. Optical studies revealed a gradual narrowing of the bandgap values from 2.81 eV (undoped) to 2.74 eV, 2.69 eV, and 2.64 eV for 0 at%, 1 at%, and 3 at% Al-doping levels, respectively. Furthermore, gas sensing tests demonstrated that higher Al doping increased resistance and reduced sensitivity toward NO_2 gas due to enhanced charge carrier recombination and altered surface interactions, indicating significant influence on semiconductor gas sensing properties.

1 INTRODUCTION

Iron oxide thin films (Fe_2O_3) doped with Al (1–3 at%) were successfully deposited on glass substrates at 400 °C using the chemical spray pyrolysis (CSP) technique [1], [2] - [5]. Iron oxides exist in different stoichiometries and crystalline forms, including FeO, Fe_3O_4, α-Fe_2O_3, and γ-Fe_2O_3, with hematite (α-Fe_2O_3) being the most stable phase [6] - [9]. Its favorable properties such as non-toxicity, low cost, and wide availability make it highly suitable for numerous applications [10] - [12].

The structural analysis by X-ray diffraction (XRD) confirmed the formation of α-Fe_2O_3 with a dominant (104) reflection, indicating high crystallinity. The average crystallite size increased from 15.82 nm to 18.70 nm with rising Al concentration, while the lattice strain decreased from 2.18 to 1.85, suggesting improved crystal quality. Atomic force microscopy (AFM) revealed a reduction in surface roughness and a more uniform particle distribution, with average particle sizes ranging from 65.5 nm to 52.31 nm.

Optical characterization showed a progressive narrowing of the optical bandgap from 2.81 eV (undoped) to 2.74 eV, 2.69 eV, and 2.64 eV for 0 at%, 1 at%, and 3 at% Al doping, respectively [19], [20]. Since the ionic radii of Al^{3+} (0.675 Å) and Fe^{3+} (0.69 Å) are close, partial substitution of Fe^{3+} by Al^{3+} is expected, influencing both the structural and optical properties of the films.

Gas sensing studies demonstrated that higher Al doping increased electrical resistance and reduced sensitivity toward NO_2 due to enhanced charge carrier recombination and modified surface interactions [10] - [14]. While various preparation techniques such as sol–gel [15], electrodeposition [16], sonochemical methods [17], and electrospinning [18] have also been employed for Fe_2O_3 films [19] - [22], CSP remains an efficient and attractive approach for large-

area deposition and detailed characterization [23], [21] - [24].

2 EXPERIMENTAL

Thin films of Fe_2O_3: Al is prepared by (CSP) technique. 0.1 M of both $AlCl_2$ and $FeCl_3$ diluted with redistilled. Al 1% and 3% was utilized. The deposition circumstances were: spray time 8 s and then stopped 1 min. The carrier gas used was air, with a pressure of 10^5 Pa, and the distance between the spout and the base was 28 cm ± 1 cm. Film thickness was found to be 325 ± 30 nm. XRD analysis verified the formation of a Fe_2O_3 thin film, and AFM is used to determine film shape. Transmittance was done via a spectrophotometer. Undoped and Al-doped Fe_2O_3 gas sensors were tested for sensitivity by resistance change in a 7.5×15 cm cylindrical chamber.

3 RESULTS AND DISCUSSION

XRD spectra of Fe_2O_3Al films are displayed in Figure 1. ICDD card no. 40-1139 and 39-1364 was fitted with the obtained data. Diffraction peaks correspond to (221), (104) and (116) planes. The shift in peak position is that the ionic radius of Al^{3+} is less than that of Fe^{3+} (0.53 Å compared to 0.69Å) [25]. The sharp and intense diffraction peaks are clearly indexed to the α-Fe_2O_3 crystalline phase.

The average crystallite size (D) is offered via Scherrer (1) [26]:

$$D = \frac{0.9\lambda}{\beta cos\theta}. \quad (1)$$

Where θ is Bragg angle, β is FWHM, and λ is X-ray wavelength. *D* are in range of 15–18 nm. The strain ε is obtained by utilizing the following by (2) [27]:

$$\varepsilon = \frac{\beta cos\theta}{4}. \quad (2)$$

The dislocation density δ is obtained by the following relation [28]

$$\delta = \frac{1}{D^2}. \quad (3)$$

It is mentioned that as Al content increases, δ and ε decrease and is assigned to the variation in ionic radii of Al^{3+} and Fe^{3+} as shown in Figure 2 c and d. the crystallite size is decreased; however, after doping, there is large crystallites that agree with [30], [32]. The values for *D* and ε are given in Table 1. A slight increase in *D* and a decrease in ε. These results agree with [33], [34]. The structural parameters are calculated and listed in Table 1.

AFM images of the grown films are offered in Figure 3, offering films uniformity. The Average Particle size P_{av} is seen as 65.5 nm, 58.7 nm and 52.3 nm for the concentration of 0%, 1% and 3%, respectively. Generally, the roughness R_a of films in the area of 8.4-4.8 nm. The undoped film surface exhibits a larger root-mean-square (rms) roughness of 9.4 nm. However, rms and R_a decrease is seen for 1% and 3% Al. Similar result is noticed in [35], [36]. The summary of the surface topography S_T is shown in Table 2.

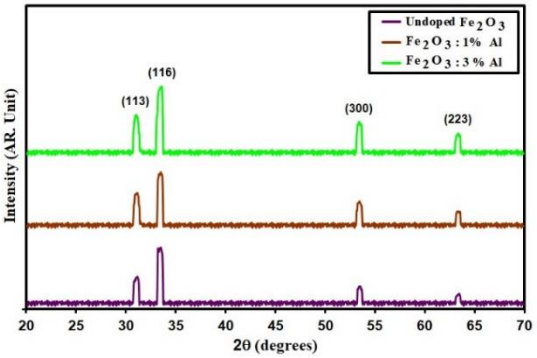

Figure 1: XRD patterns of of Undoped and Fe_2O_3: Al films.

Table 1: Structure parameters of Undoped and Fe_2O_3: Al films.

Samples	(hkl) Plane	2□ (º)	FWHM (º)	E_g eV	*D* nm	δ X(10^{15})(line/m^2)	ε (×10^{-3})
Undoped Fe_2O_3	104	33.82	0.51	2.74	15.8	3.9	2.1
Fe_2O_3: 1% Al	104	33.79	0.48	0.69	17.1	3.4	2.0
Fe_2O_3: 3% Al	104	33.74	0.44	2.64	18.7	2.8	1.8

Table 2: The Morphological values of Undoped and Fe_2O_3: Al films.

Samples	P_{av},nm	R_a, nm	R_{ms}, nm
Undoped Fe_2O_3	65.5	8.7	9.4
Fe_2O_3: 1% Al	58.7	6.3	8.7
Fe_2O_3: 3% Al	52.3	4.8	5.4

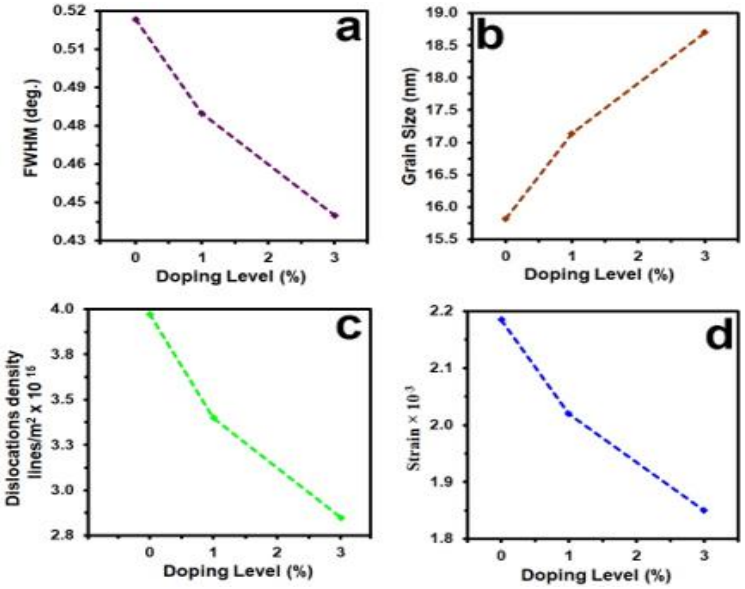

Figure 2: X-ray parameter of Undoped and Fe_2O_3: Al films.

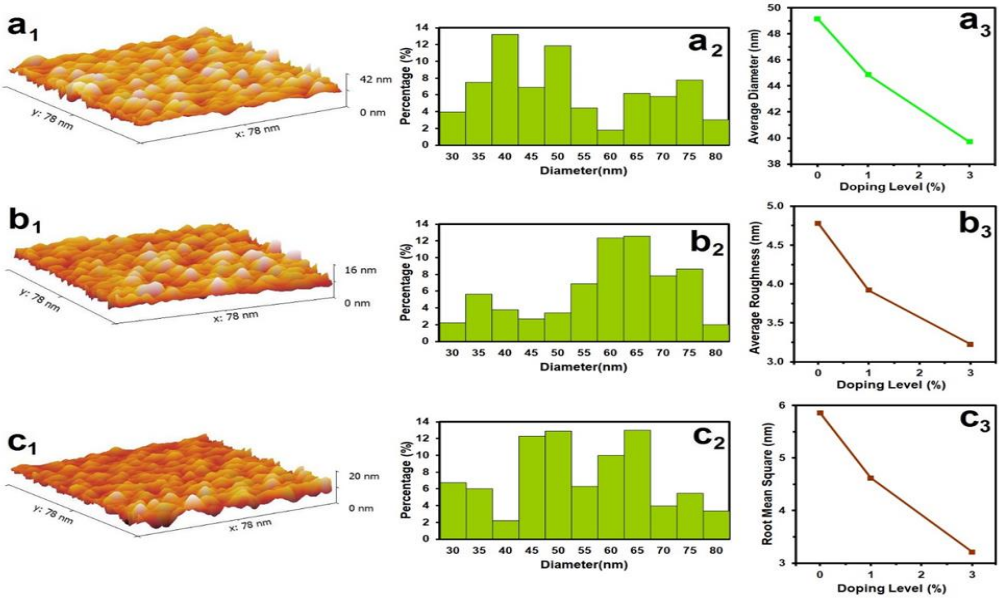

Figure 3: AFM images of Undoped and Fe2O3: Al films.

The transmittance T of the intended films is displayed in Figure 4. Films have a transparency of 65 %. From Figure 4. The doping decreases T, which refers to strong scattering and absorption [37], [38]. The drop in T with increasing Al content can be assigned to the surrogate of Fe+3 by Al^{+3}, which reduces light in the T band. This behavior is similar to that observed in [39], [40].

The absorption coefficient (α) was evaluated using the optical transmittance spectra. α is calculated using (4) [41]:

$$\alpha = \frac{1}{d} ln \frac{I_0}{I} = 2.303(\frac{A}{d}), \quad (4)$$

where d is film thickness. Figure 5 shows α versus the photon energy ($h\nu$) of various doping of Al. High

α between 1×10^4cm^{-1}and 6×10^4 cm^{-1} in the visible area. Also, we note that the α increased with film doping increasing.

Optical bandgap, denoted by (5) is computed employing the relation below [42]:

$$(\alpha hv) = A\left(hv - E_g\right)^n, \quad (5)$$

where A is constant and n = ½, for allowed direct transitions. Figure 6. shows E_g values determined as 2.74, 2.69 and 2.64, 2.81 at 0.at%, 1 at% and 3 at% of Al respectively. This decrease in bandgap indicates that Al provides Al^{3+} ions [43], [44].

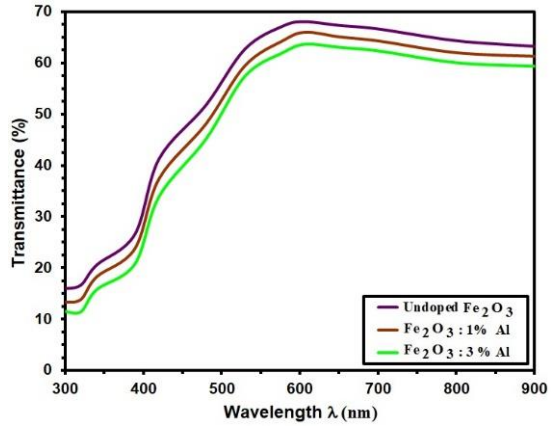

Figure 4: Transmittance of Undoped and Fe_2O_3: Al films.

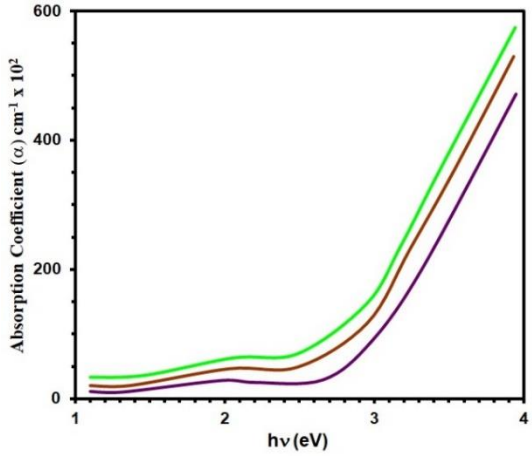

Figure 5: Absorption coefficient (α) of Undoped and Fe_2O_3: Al films.

The formula below [36] evaluates the extinction coefficient (k) [45, 46]:

$$k = \frac{\alpha\lambda}{4\pi}. \quad (6)$$

k against wavelength is shown in Figure 7. There is a decrease k in the visible area of 550-700 nm**,** then a rapid rise within the 400-500 nm area. k increasing with Al content and arriving at the highest value at 3wt% content, this increase is related to an increase in carrier concentration in CB according to Burstein-Moss effect [47], [48].

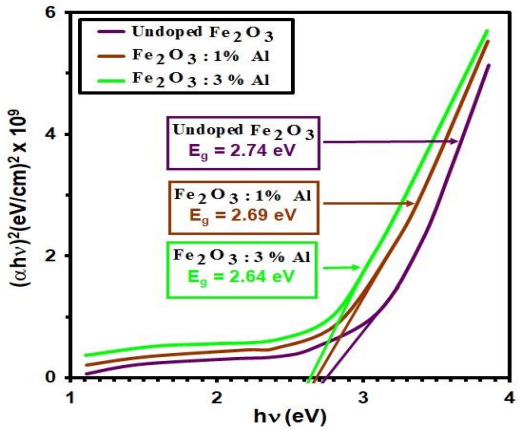

Figure 6: Optical bandgap (Eg) of Undoped and Fe_2O_3: Al films

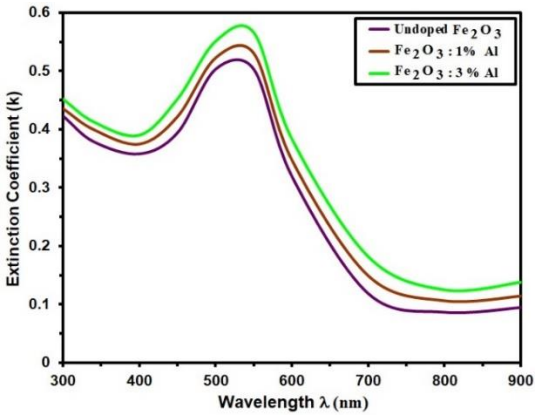

Figure 7: Extinction coefficient (k) of Undoped and Fe_2O_3: Al films.

The refractive index (n) is obtained by the relation [49]:

$$n = \frac{1+R^{\frac{1}{2}}}{1-R^{\frac{1}{2}}}. \quad (7)$$

Figure 8 offers n plotted via wavelength. The values n is in the area of 3.5–3.75 and are almost constant at longer wavelengths. It can be assigned to film polarization [40], [51]. These results assure using this composite as a window layer of solar cell [52], [53].

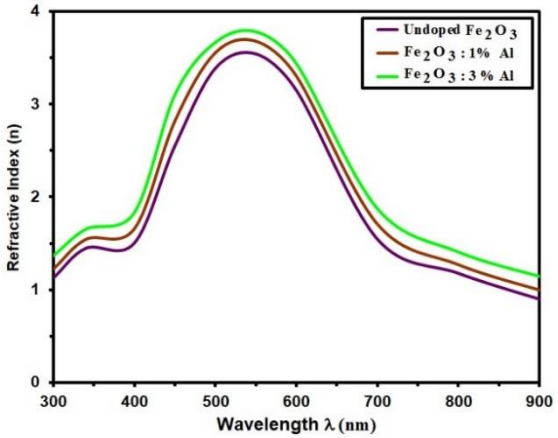

Figure 8: Refractive index (n) of Undoped and Fe_2O_3: Al films.

Figure 9 shows increased resistance over time for undoped and Al-doped Fe_2O_3 films exposed to 300 ppm NO_2 at 150 °C, indicating surface oxidation during gas exposure [54], [55]. NO_2 adsorption on Fe_2O_3 films removes O2+ ions, releasing electrons to the conduction band and increasing resistance. Al doping, especially at 4%, significantly enhances resistance, demonstrating its strong effect on sensing and semiconductor properties[56] - [58].

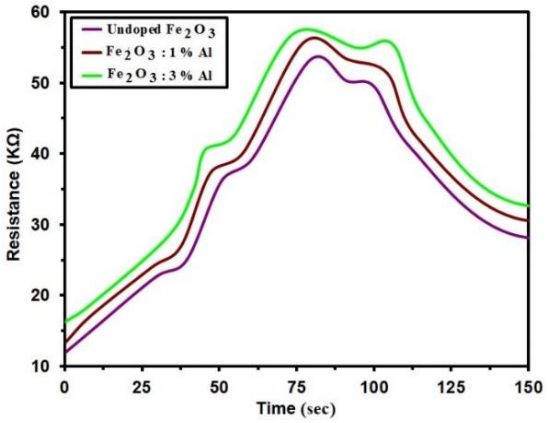

Figure 9: The variation of resistance over time for Fe2O3 and Al-doped Fe2O3 films.

Sensitivity (S) is is calculated using the following (8) [59]:

$$Sensitivity = \frac{\Delta R}{R_g} = \left|\frac{R_g - R_a}{R_g}\right| \times 100\ \%\ . \quad (8)$$

Figure 10 shows reduced sensitivity with higher Al content due to increased resistance from charge carrier recombination after NO_2 exposure. Increasing Al doping leads to greater charge carrier recombination, reducing conductivity and gas response [60]. Sensitivity drops significantly at higher doping levels, indicating suppressed NO_2 sensing performance of Fe_2O_3 films due to reduced free carrier availability [61].

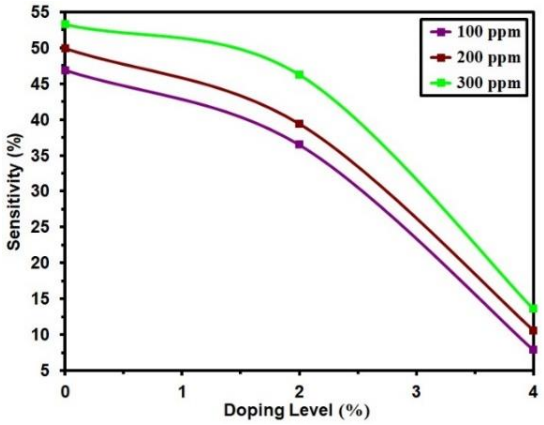

Figure 10: Sensitivity (S) as a function of Al-doped Fe_2O_3 films at different concentrations.

4 CONCLUSIONS

Aluminum-doped iron oxide (Fe_2O_3:Al) thin films were successfully synthesized using the chemical spray pyrolysis (CSP) technique at a substrate temperature of 400°C. Structural analysis confirmed the formation of a well-crystallized α-Fe_2O_3 phase across all doping levels, with enhanced crystallinity observed at 3 at% Al. The incorporation of Al^{3+} ions led to a slight increase in crystallite size and a reduction in lattice strain and dislocation density. Morphological analysis revealed that increasing Al content resulted in more uniform surface morphology, reduced particle size, and lower surface roughness, as confirmed by AFM measurements. These improvements are beneficial for optical and electronic applications. Optical characterization showed that the transmittance and optical bandgap (Eg) decreased with increasing Al doping, while the extinction coefficient (k) and refractive index (n) increased. The bandgap narrowing is attributed to enhanced carrier concentration and Al^{3+} substitution effect. Gas sensing performance tests indicated that while Al doping improved film crystallinity and morphology, it adversely affected sensitivity to NO_2 gas. Higher Al concentrations led to increased resistance and suppressed sensor response due to enhanced charge carrier recombination and reduced availability of free carriers.

ACKNOWLEDGMENTS

The authors would like to express their gratitude to Mustansiriyah University and Al-Nukhba University College for their support.

REFERENCES

[1] T. Mariño-Otero, M. Oliver-Tolentino, M. A. Aguilar-Frutis, G. Contreras-Martínez, E. Pérez-Cappe, and E. Reguera, "Effect of thickness in hematite films produced by spray pyrolysis towards water photo-oxidation in neutral media," Int. J. Hydrogen Energy, vol. 40, pp. 5831-5836, 2015, [Online]. Available: https://doi.org/10.1016/J.IJHYDENE.2015.03.017.

[2] S. A. J. Al-Dahaan, A. H. O. Al-khayatt, and M. K. Salman, "The optical properties of Fe_2O_3 thin film prepared by chemical spray pyrolysis deposition (CSP)," J. Kufa Phys., vol. 6, no. 2, pp. 16-23, 2014.

[3] A. A. Akl, "Thermal annealing effect on the crystallization and optical dispersion of sprayed V_2O_5 thin films," J. Phys. Chem. Solids, vol. 71, pp. 223-229, 2010.

[4] A. S. Hassanien and A. A. Akl, "Microstructure and crystal imperfections of nano-crystalline sprayed iridium oxides thin films," Physica B, vol. 473, pp. 11-19, 2015.

[5] A. A. Akl, S. A. Mahmoud, S. M. Al-Shomar, and A. S. Hassanien, "Improving microstructural properties and minimizing crystal imperfections of nanocrystalline Cu_2O thin films of different solution molarities for solar cell applications," Mater. Sci. Semicond. Process., vol. 74, pp. 183-192, 2018.

[6] M. F. Al-Kuhaili, M. Saleem, and S. M. A. Durrani, "Optical properties of iron oxide (α-Fe_2O_3) thin films deposited by the reactive evaporation of iron," J. Alloy. Compd., vol. 521, p. 178, 2012.

[7] 7 H. Mansour, H. Letifi, R. Bargougui, S. De Almeida-Didry, B. Negulescu, C. A. Lambert, A. Gadri, and S. Ammar, "Structural, optical, magnetic and electrical properties of hematite (α-Fe_2O_3) nanoparticles synthesized by two methods: polyol and precipitation," Appl. Phys. A, vol. 123, p. 787, 2017, doi:10.1007/s00339-017-1408-1.

[8] J. Singh, S. Khan, J. Shah, R. Kotnala, and S. Mohapatra, "Nanostructured TiO_2 thin films prepared by RF magnetron sputtering for photocatalytic applications," Appl. Surf. Sci., vol. 422, pp. 953-961, 2017, [Online]. Available: https://doi.org/10.1016/J.APSUSC.2017.06.068.

[9] Z. Hubička, Š. Kment, J. Olejníček, M. Čada, T. Kubart, M. Brunclíková, P. Kšírová, P. Adámek, and Z. Remeš, "Deposition of hematite Fe_2O_3 thin film by DC pulsed magnetron and DC pulsed hollow cathode sputtering system," Thin Solid Films, vol. 549, pp. 184-191, 2013, [Online]. Available: https://doi.org/10.1016/J.TSF.2013.09.031.

[10] E. L. Miller, D. Paluselli, B. Marsen, and R. E. Rocheleau, "Low-temperature reactively sputtered iron oxide for thin film devices," Thin Solid Films, vol. 466, pp. 307-313, 2004, [Online]. Available: https://doi.org/10.1016/J.TSF.2004.02.093.

[11] B. Issa, I. M. Obaidat, B. A. Albiss, and Y. Haik, "Magnetic nanoparticles: Surface effects and properties related to biomedicine applications," Int. J. Mol. Sci., vol. 14, no. 11, pp. 21266-21305, 2013, doi:10.3390/ijms141121266.

[12] D. Lee, J. Kim, T. Han, J. Hwang, S. Jeon, S. Choi, S. Hong, W. Lee, R. Ruoff, and S. Kim, "Versatile carbon hybrid films composed of vertical carbon nanotubes grown on mechanically compliant graphene films," Adv. Mater., vol. 22, 2010, [Online]. Available: https://doi.org/10.1002/adma.200903063.

[13] S. Shinde, A. Moholkar, J. Kim, and K. Rajpure, "Structural, morphological, luminescent and electronic properties of sprayed aluminium incorporated iron oxide thin films," Surf. Coat. Technol., vol. 205, pp. 3567-3577, 2011, [Online]. Available: https://doi.org/10.1016/J.SURFCOAT.2010.12.022.

[14] A. Kleiman-Shwarsctein, M. N. Huda, A. Walsh, Y. Yan, G. D. Stucky, Y.-S. Hu, M. M. Al-Jassim, and E. W. McFarland, "Electrodeposited aluminum-doped α-Fe_2O_3 photoelectrodes: experiment and theory," Chem. Mater., vol. 22, pp. 510-517, 2010, [Online]. Available: https://doi.org/10.1021/cm903135j.

[15] W. B. Ingler Jr and S. U. M. Khan, "Photoresponse of spray pyrolytically synthesized magnesium-doped iron(III) oxide (p-Fe_2O_3) thin films under solar simulated light illumination," Thin Solid Films, vol. 461, pp. 301-308, 2004.

[16] K. H. Abass, "Fe_2O_3 thin films prepared by spray pyrolysis technique and study the annealing on its optical properties," Int. Lett. Chem. Phys. Astron., vol. 6, pp. 24-31, 2015.

[17] J. Krysa, M. Zlamal, S. Kment, M. Brunclíková, and Z. Hubička, "TiO_2 and Fe_2O_3 films for photoelectrochemical water splitting," Molecules, vol. 20, no. 1, p. 1046, 2015.

[18] R. Schrebler, K. Bello, F. Vera, P. Cury, E. Muñoz, R. del Rio, H. G. Meier, R. Cordova, and E. A. Dalchiele, "An electrochemical deposition route for obtaining α-Fe_2O_3 thin films," Electrochem. Solid-State Lett., vol. 9, 2006, [Online]. Available: https://doi.org/10.1149/1.2200141.

[19] R. Kumar, Y. Diamant, and A. Gedanken, "Sonochemical synthesis and characterization of nanometer-size transition metal oxides from metal acetates," Chem. Mater., vol. 12, pp. 2301-2305, 2000, [Online]. Available: https://doi.org/10.1021/CM000166Z.

[20] G. Binitha, M. Soumya, A. A. Madhavan, P. Praveen, A. Balakrishnan, K. Subramanian, M. Reddy, S. V. Nair, A. S. Nair, and N. Sivakumar, "Electrospun α-Fe_2O_3 nanostructures for supercapacitor applications," J. Mater. Chem., vol. 1, pp. 11698-11704, 2013, [Online]. Available: https://doi.org/10.1039/C3TA12352A.

[21] A. Todorovska, S. Groudeva-Zotova, and D. Todorovsky, "Spray pyrolysis deposition of α-Fe_2O_3 thin films using iron(III) citric complexes," Mater. Lett., vol. 56, pp. 770-774, 2002, [Online]. Available: https://doi.org/10.1016/S0167-577X(02)00611-0.

[22] S. Kulkarni and C. Lokhande, "Structural, optical, electrical and dielectrical properties of electrosynthesized nanocrystalline iron oxide thin films," Mater. Chem. Phys., vol. 82, pp. 151-156, 2003, [Online]. Available: https://doi.org/10.1016/S0254-0584(03)00212-8.

[23] A. A. Akl, "Microstructure and electrical properties of iron oxide thin films deposited by spray pyrolysis," Appl. Surf. Sci., vol. 221, pp. 319-329, 2004, [Online]. Available: https://doi.org/10.1016/S0169-4332(03)00951-6.

[24] A. Ali, H. Zafar, M. Zia, I. ul Haq, A. R. Phull, J. S. Ali, and A. Hussain, "Synthesis, characterization, applications, and challenges of iron oxide nanoparticles," Nanotechnol., Sci. Appl., vol. 9, pp. 49-67, 2016, [Online]. Available: https://doi.org/10.2147/NSA.S99986.

[25] V. Chernyshova, M. F. Hochella Jr, and A. S. Madden, "Size-dependent structural transformations of hematite nanoparticles. 1. Phase transition," Phys. Chem. Chem. Phys., vol. 9, p. 1736, 2007.

[26] S. S. Chiad, H. A. Noor, O. M. Abdulmunem, and N. F. Habubi, "Optical and structural properties of Ni-doped Co_3O_4 nanostructure thin films via CSPM," J. Phys.: Conf. Ser., vol. 1362, no. 1, 2019.

[27] P. Malliga, J. Pandiarajan, N. Prithivikumaran, and K. Neyvasagam, "Influence of film thickness on structural and optical properties of sol-gel spin coated TiO_2 thin film," IOSR J. Appl. Phys., vol. 6, pp. 22-28, 2014, [Online]. Available: https://doi.org/10.9790/4861-06112228.

[28] G. K. Williamson and R. E. Smallman, "Dislocation densities in some annealed and cold-worked metals from measurements on the X-ray Debye-Scherrer spectrum," Philos. Mag., vol. 1, no. 1, pp. 34-45, 1956, doi:10.1080/14786435608238074.

[29] U. Schwertmann, R. W. Fitzpatrick, R. M. Taylor, and D. G. Lewis, "The influence of aluminum on iron oxide. Part II. Preparation and properties of Al-substituted hematites," Clays Clay Miner., vol. 27, no. 2, pp. 105-112, 1979.

[30] D. G. Schulze and U. Schwertmann, "The influence of aluminum on iron oxides. XIII. Properties of goethites synthesized in 0.3 M KOH at 25°C," Clay Miner., vol. 22, pp. 83-92, 1987.

[31] M. R. Belkhedkar, A. U. Ubale, Y. S. Sakhare, N. Zubair, and M. Musaddique, "Characterization and antibacterial activity of nanocrystalline Mn doped Fe_2O_3 thin films grown by successive ionic layer adsorption and reaction method," J. Assoc. Arab Univ. Basic Appl. Sci., vol. 21, pp. 38-44, 2016.

[32] Y. H. Elbashar and H. A. Abd El-Ghany, "Optical spectroscopic analysis of Fe_2O_3 doped CuO containing phosphate glass," Opt. Quant. Electron., vol. 49, p. 310, 2017.

[33] A. K. Varshneya, Fundamentals of Inorganic Glasses, San Diego: Academic Press, 1994.

[34] W. Wenjian, M. Ming, P. Du, Z. Gaoling, S. Ge, W. Jianxun, and H. Gaorong, "Super-hydrophilic Fe-doped titanium dioxide thin films prepared by a spray pyrolysis deposition," Surf. Coat. Technol., vol. 198, pp. 340-344, 2005.

[35] E. F. Keskenler, G. Turgut, and S. Dogan, "Investigation of structural and optical properties of ZnO films co-doped with fluorine and indium," Superlattices Microstruct., vol. 52, pp. 107-115, 2012.

[36] J. I. Pankov, Optical Processes in Semiconductors, 1971.

[37] J. Kaur and M. Sharma, "Structural and optical studies of undoped and copper doped zinc sulphide nanoparticles for photocatalytic application," Superlattices Microstruct., vol. 77, pp. 35-53, 2015.

[38] J. Simmons and K. S. Potter, Optical Materials, 1st ed., New York: Academic Press, 1999.

[39] Y. A. Al Shaabani, "Studying some physical properties of $Zn_{2x}Cu_{1-x}In_{1-x}S_2$ thin films prepared by chemical spray pyrolysis," Appl. Sci. Univ. of Technology, 2009.

[40] M. A. Kaid and A. Ashour, "Preparation of ZnO-doped Al films by spray pyrolysis technique," Appl. Surf. Sci., vol. 253, pp. 3029-3033, 2007.

[41] S. S. Chiad, A. S. Alkelaby, and K. S. Sharba, "Optical conduct of nanostructure Co_3O_4 rich highly doping Co_3O_4:Zn alloys," J. Glob. Pharma Technol., vol. 11, no. 7, pp. 662-665, 2020.

[42] X. W. Li, A. Gupta, G. Xiao, and G. Q. Gong, "Transport and magnetic properties of epitaxial and polycrystalline magnetite thin films," J. Appl. Phys., vol. 83, pp. 7049-7051, 1998.

[43] A. Z. Moshfegh, R. Azimirad, and O. Akhavan, "Optical properties and surface morphology of evaporated $(WO_3)_{1-x}$–$(Fe_2O_3)_x$ thin films," Thin Solid Films, vol. 484, pp. 124-131, 2005.

[44] J. A. Glasscock, P. R. F. Barnes, I. C. Plumb, and N. Savvides, "Enhancement of photoelectrochemical hydrogen production from hematite thin films by the introduction of Ti and Si," J. Phys. Chem. C, vol. 111, pp. 16477-16488, 2007.

[45] A. A. Khadayeir, R. I. Jasim, S. H. Jumaah, N. F. Habubi, and S. S. Chiad, "Influence of substrate temperature on physical properties of nanostructured ZnS thin films," J. Phys.: Conf. Ser., vol. 1664, no. 1, 2020.

[46] R. S. Ali, M. K. Mohammed, A. A. Khadayeir, Z. M. Abood, N. F. Habubi, and S. S. Chiad, "Structural and optical characterization of sprayed nanostructured indium doped Fe_2O_3 thin films," J. Phys.: Conf. Ser., vol. 1664, no. 1, p. 012016, 2020.

[47] A. B. F. Martinson, M. J. DeVries, J. A. Libera, S. T. Christensen, J. T. Hupp, M. J. Pellin, and J. W. Elam, "Atomic layer deposition of Fe_2O_3 using ferrocene and ozone," J. Phys. Chem. C, vol. 115, pp. 4333-4339, 2011.

[48] R. S. Ali, N. A. H. Al-Aaraji, E. H. Hadi, K. H. Abass, N. F. Habubi, and S. S. Chiad, "Effect of lithium on structural and optical properties of nanostructured CuS thin films," J. Nanostruct., vol. 10, no. 4, pp. 810-816, 2020, doi:10.22052/JNS.2020.04.014.

[49] J. Park, S. Kim, and A. J. Bard, "Novel carbon-doped TiO_2 nanotube arrays with high aspect ratios for efficient solar water splitting," Nano Lett., vol. 6, no. 1, pp. 24-28, 2006, [Online]. Available: https://doi.org/10.1021/NL051807Y.

[50] .M. Matsuoka, M. Kitano, M. Takeuchi, K. Tsujimaru, M. Anpo, and J. Thomas, "Photocatalysis for new energy production: recent advances in photocatalytic water splitting reactions for hydrogen production," Catal. Today, vol. 122, pp. 51-61, 2007, [Online]. Available: https://doi.org/10.1016/J.CATTOD.2007.01.042.

[51] S. Wang, W. Wang, W. Wang, Z. Jiao, J. Liu, and Y. Qian, "Characterization and gas-sensing properties of nanocrystalline iron(III) oxide films prepared by ultrasonic spray pyrolysis on silicon," Sens. Actuators B Chem., vol. 69, pp. 22-27, 2000.

[52] E. Lee, G. Jang, C. Kim, and D. Yoon, "Fabrication and gas sensing properties of α-Fe_2O_3 thin film prepared by plasma enhanced chemical vapor deposition (PECVD)," Sens. Actuators B Chem., vol. 77, pp. 221-227, 2001.

[53] Q. Hao, L. Li, X. Yin, S. Liu, Q. Li, and T. Wang, "Anomalous conductivity-type transition sensing behaviors of n-type porous α-Fe_2O_3 nanostructures toward H_2S," Mater. Sci. Eng. B, vol. 176, pp. 600-605, 2011.

[54] K. L. Hardee and A. J. Bard, "Semiconductor electrodes. 10. Photoelectrochemical behavior of several polycrystalline metal-oxide electrodes in aqueous solutions," J. Electrochem. Soc., vol. 124, p. 215, 1977.

[55] P. Scherrer, "Über die Berechnung der Größe und der inneren Struktur von Kolloidteilchen mittels Röntgenstrahlen," Nachrichten Ges. Wiss. Göttingen, Math.-Phys. Kl., vol. 2, pp. 98-100, 1918.

[56] C. D. Park, D. Magana, and A. E. Stiegman, "High-quality Fe and γ-Fe_2O_3 magnetic thin films from an epoxide-catalyzed sol–gel process," Chem. Mater., vol. 19, pp. 677-683, 2007.

[57] R. M. Cornell and U. Schwertmann, The Iron Oxides: Structure, Properties, Reactions, Occurrences and Uses, 2nd ed., Weinheim: Wiley-VCH, 2003.

[58] H. T. Salloom, E. H. Hadi, N. F. Habubi, S. S. Chiad, M. Jadan, and J. S. Addasi, "Characterization of silver content upon properties of nanostructured nickel oxide thin films," Digest J. Nanomater. Biostruct., vol. 15, no. 4, pp. 1189-1195, 2020.

[59] N. Khademi and M. M. Bagheri-Mohagheghi, "The structural, thermoelectric and optical properties of SnO_2-Fe_2O_3:Bi thin films deposited by spray prol(y)sis technique," Thermal Energy Power Eng., vol. 2, pp. 89-93, 2013.

[60] J. S. Corneille, J.-W. He, and D. W. Goodman, "Preparation and characterization of ultra-thin iron oxide films on a Mo(100) surface," Surf. Sci., vol. 338, no. 1, pp. 211-224, 1995.

[61] J. Krysa, M. Zlamal, S. Kment, and Z. Hubicka, "Photo-electrochemical properties of WO_3 and α-Fe_2O_3 thin films," Proc. Italian Assoc. Chem. Eng., vol. 41, pp. 379-484, 2014.